JOURNAL OF SOLID STATE CHEMISTRY 56, 318–324 (1985)

High-Resolution Electron Microscopic Study of V_6O_{13}

T. OHNO,* Y. NAKAMURA, AND S. NAGAKURA

Department of Metallurgy, Tokyo Institute of Technology, Oh-okayama, Meguro-ku, Tokyo 152, Japan

Received March 26, 1984; in revised form July 2, 1984

High-resolution structure images of V_6O_{13} were taken with a 1-MV electron microscope with a cutoff resolution of 0.14 nm. Individual V atom rows, as well as tunnels in the structure, were resolved. The effect of the electronic state on the structure image was investigated by comparing the observed image with the simulated images calculated by assuming various ionized states to the constituent atoms. The neutral-state model interpreted the observed image more satisfactorily than the ionized-state models. A modification of V_6O_{13} was displayed as an image. In order to interpret the image, a structure model was proposed, which is orthorhombic with lattice parameters $a = 1.1922$, $b = 1.9912$, and $c = 0.3680$ nm and belongs to the space group *Cmma*. This structure is derived from the V_2O_5 structure by removing all the atoms on every third (001) oxygen atom plane and then introducing crystallographic shear $\frac{1}{2}[01\bar{1}\,1]$, instead of $\frac{1}{6}[103]$ in the case of normal V_6O_{13}.

Introduction

In the vanadium–oxygen system, there are many line phases called Magnéli phases. Between V_2O_3 and VO_2 the line phases are generally expressed as V_nO_{2n-1} (n = 2–9, ∞) (*1*), and between VO_2 and V_2O_5, they are as $V_{2n}O_{5n-2}$ (*2*) or V_nO_{2n+1} (n = 2, 3, 4, 6, ∞) (*3*). For V_nO_{2n-1}, especially for V_6O_{11} and V_7O_{13}, Hirotsu *et al.* (*4–6*) observed the crystallographic shear (*CS*) structures and the microsyntactic intergrowth of several phases with neighboring n on the unit cell scale by high-resolution electron microscopy. As a succession of these studies, the present study was made for V_6O_{13} belonging to the group V_nO_{2n+1}.

The crystal structure of V_6O_{13} was analyzed by Aebi (*7*) and refined by Wilhelmi *et al.* (*8*). The structure is monoclinic and can be derived from the structure of V_2O_5 (*9*) by removing all the atoms on every third (001) oxygen atom plane and then introducing the *CS* of $\frac{1}{6}[10\bar{3}]$. Figures 1a and b show, respectively, the [010] projection of the V_2O_5 and V_6O_{13} structures in an idealized form, where VO_6 octahedra link together by sharing their corners and edges. Every V atom is displaced appreciably from the center of the octahedron.

High-resolution electron microscopic observations of V_6O_{13} have been made by Horiuchi *et al.* (*11, 12*) by using 100-kV and 1-MV electron microscopes. They succeeded in resolving the individual VO_6 octahedra. They also observed the phase transition of V_6O_{13} to VO_2 induced by electron irradiation (*11*). In the present study, we succeeded in resolving individual V atom rows in the structure. The effect of electronic state on the structure image was investi-

* Present address. Hitachi Research Laboratory, Hitachi Ltd., Hitachi-shi, Ibaraki, Japan.

0022-4596/85 $3.00

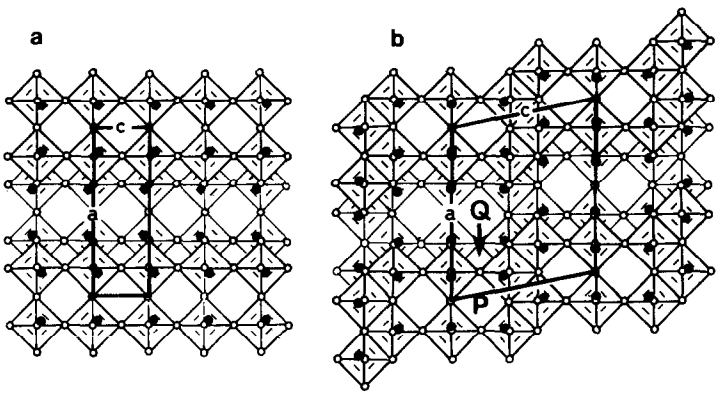

FIG. 1. Idealized structure of (a) V_2O_5 and (b) V_6O_{13}. [010] projections. Solid circles: V atoms. Open circles: O atoms. In (b), P and Q are tunnels formed among the VO_6 octahedra. Lattice parameters and space group: V_2O_5 $a = 1.1510$, $b = 0.3563$, $c = 0.4369$ nm, *Pmmn*; V_6O_{13} $a = 1.1922$, $b = 0.3680$, $c = 1.0138$ nm, $\beta = 100.87°$, *C2/m*.

gated. A modification of V_6O_{13} was observed and its structure model was proposed. These are described in this paper.

Experimental

Polycrystalline V_6O_{13} was produced by heating a powder mixture of V_2O_5 and V_2O_3 (mixing atom ratio V : O = 6 : 13) sealed in a quartz capsule at 670°C for 3 days. Raw materials used were commercial V_2O_5 powder (purity 99.9%) and V_2O_3 powder, prepared by reducing commercial V_2O_5 powder in a hydrogen stream at 800°C for 3 days. An X-ray diffraction investigation identified the produced polycrystalline material with V_6O_{13}. The V_6O_{13} sample thus prepared was crushed in acetone, and fine flakes produced were scooped on a microgrid for use on electron microscopy.

Electron microscopes used are a JEM-200CX operating at 200 kV (cutoff resolution 0.29 nm) and the Ultrahigh-Vacuum High-Resolution 1-MV Electron Microscope (UHV-HR-1 MV EM, cutoff resolution 0.14 nm) recently installed at Tokyo Institute of Technology (*12, 13*). Structure images were usually taken under the optimum defocus condition. In order to explain the recorded images, image simulation were made by applying the multislice method (*14*). In Table I, the standard imaging and simulation conditions are shown.

Results

a. Structure Image of V_6O_{13}

Figure 2a reproduces a structure image of V_6O_{13} taken with the UHV-HR-1 MV EM and Fig. 2b the corresponding selected area electron diffraction pattern. The incident

TABLE I

IMAGING AND SIMULATION CONDITIONS

Item	200-kV EM	1-MV EM
Wavelength	2.51×10^{-3} nm	0.872×10^{-3} nm
No. excited waves	1025	1519
No. imaging waves for simulation	37	89
Objective aperture used ($\sin\theta/\lambda$)	2 nm^{-1}	3.8 nm^{-1}
Spherical aberration coefficient of objective lens	2.5 mm	2.5 mm
Width of chromatic aberration	10 nm	15 nm
Cutoff resolution	0.29 nm	0.14 nm
Angle of beam divergence	7×10^{-4} rad	4×10^{-4} rad
Scherzer focus	92 nm	47 nm
No. slices	10	10
Slice thickness	0.368 nm	0.368 nm

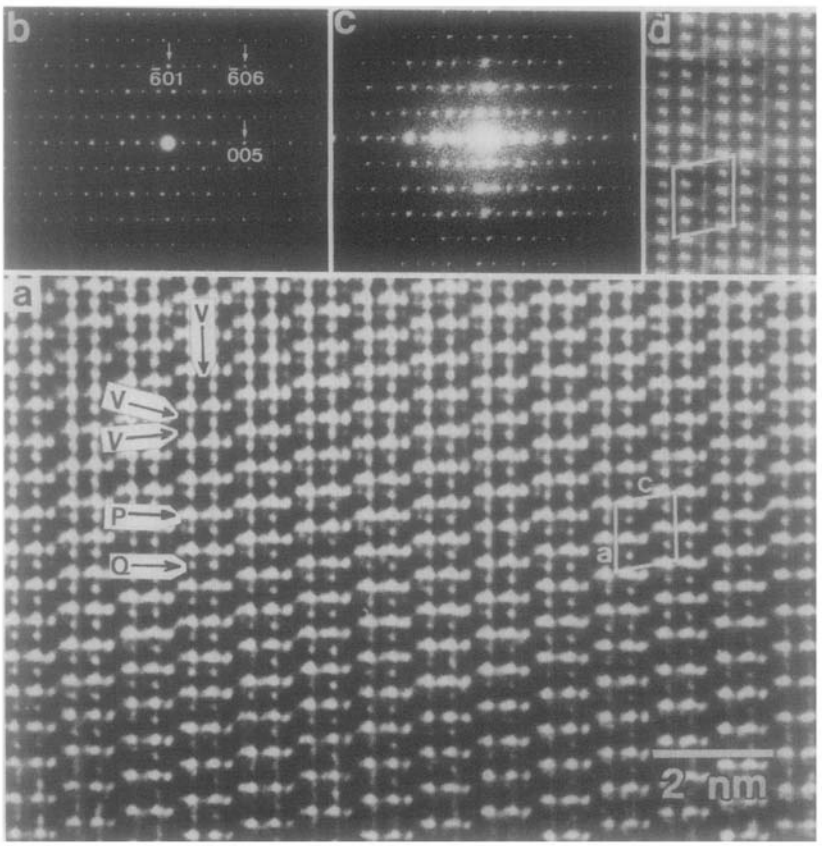

FIG. 2. (a) Structure image of V_6O_{13} taken with the UHV-HR-1 MV EM. Incident beam direction is [010]. The white dots P and Q are the images of tunnels, while the black dots V are the images of V-atom rows. (b) Selected area electron diffraction pattern. (c) Optically transformed pattern of (a), where the spots outside a circle with radius 7 nm^{-1} (not shown, passing between 007 and 008 spots) may be due to the half-spacings arising from the multiple interference of the electron waves.

beam direction is [010]. An optically transformed pattern of the recorded image is also shown in Fig. 2c. Figure 2d is a simulated image for the amount of defocus 55 nm and the crystal thickness 3.68 nm (= 10*b*). The agreement between the recorded and the simulated images is satisfactory. From the comparison of Fig. 2a with Figs. 1b and 2d, we can see that the large white dot P in Fig. 2a corresponds to the large tunnel P in Fig. 1b and the middle-sized white dot Q in Fig. 2a to the small tunnel Q in Fig. 1b. In Fig. 2a, the black dots V are observed in the vicinity of P and Q. By referring to the simulated image, the black dot V in the image can be identified with the V-atom row aligned in the [010] direction. Similarly, the small white dot adjacent to the dot P can be identified with the interstice between the V-atom rows. The rows of O atoms are not imaged. This is due to the scattering power of O atom being considerably weaker than that of V atom.

b. Effect of Electronic State on the Structure Image

The simulated image shown in Fig. 2d was obtained under the assumption that all the constituent atoms are neutral. However, there is a possibility that the constitu-

ent atoms are ionized. If V_6O_{13} is in the ideal ionized state, its electronic state may be expressed as $V(1)_2^{4+}V(2)_2^{5+}V(3)_2^{4+}O_{13}^{2-}$, where $V(1)^{4+}$, $V(2)^{5+}$, and $V(3)^{4+}$ ions are at the 4(*i*) positions in the space group *C2/m* with different parameter values (*8*).

According to the change in the electronic state, the atomic scattering factor for electrons varies considerably in the low scattering angle region smaller than $\sin\theta/\lambda = 2$ nm^{-1} (θ: Bragg angle, λ: wavelength). This fact has been used to investigate the electronic state of some interstitial compounds (*15–18*). In the present study, we made simulation calculations by assuming various ionized states to V atoms and compared the results with observed images. The imaging and the simulation were done for 200-kV electrons under a defocus value larger than the optimum one, in order to make the low-order reflections contribute effectively to the image formation, by taking the shape change in the transfer function with increasing amount of defocus into consideration.

As examples, we reproduce in Figs. 3a and b simulated images for the neutral model $V_6^0O_{13}^0$ and ideally ionized model $V_2^{4+}V_2^{5+}V_2^{4+}O_{13}^{2-}$, respectively. The amount of defocus is 116 nm and the crystal thickness is 36.8 nm. Figure 3c is a structure image taken under almost the same condition. It can be seen that the observed image resembles Fig. 3a rather than b. This shows that the use of scattering factor for the neutral atom is more appropriate than the use of that for the ionized atom for the image simulation. A similar conclusion has been obtained in the case of $W_4Nb_{26}O_{77}$ (*19*).

c. A Modification of V_6O_{13}

Some specimen flakes gave structure images as shown in Fig. 4a, where the image in the region α is the same as the image shown in Fig. 2a but the image in the region β is different. The region β does not de-

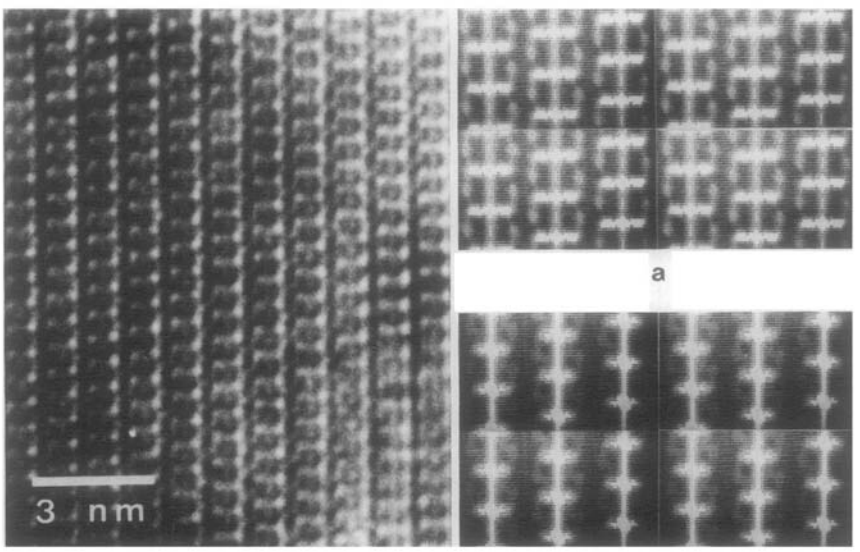

FIG. 3. Simulated images for (a) the neutral state $V_6^0O_{13}^0$ and (b) the ideally ionized state $V_2^{4+}V_2^{5+}V_2^{4+}O_{13}^{2-}$. (c) Structure image taken with 200-kV electron microscope under a defocus of 116 nm. Incident beam direction is [010].

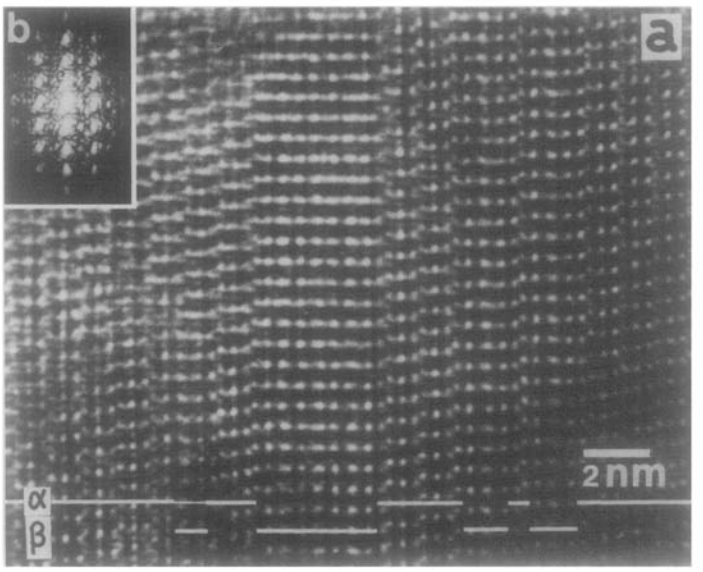

FIG. 4. (a) Structure image showing the coexistence of α-V_6O_{13} and β-V_6O_{13} taken with 1-MV electron microscope. (b) Optically transformed pattern of the region β.

velop widely, but is separated by thin α layers. Figure 4b is an optically transformed pattern of the region β.

The structure image of the region β and its optically transformed pattern can be interpreted by assuming a modification of V_6O_{13} as shown in Fig. 5a. This structure model is derived from the structure of V_2O_5 by removing all the O atoms in every third (001) oxygen atom plane and then introducing the *CS* of $\frac{1}{2}[0\bar{1}\,\bar{1}]$, instead of introducing the *CS* of $\frac{1}{6}[10\bar{3}]$ in the case of normal V_6O_{13}. In order to distinguish the two oxide forms, we refer to the normal V_6O_{13} as α and its modification as β. This β-V_6O_{13} model is orthorhombic with lattice parameters $a_\beta = 1.1922$ ($= a_\alpha$), $b_\beta = 1.9912$ ($= 2c_\alpha \sin \beta_\alpha$), and $c_\beta = 0.3680$ nm ($= b_\alpha$). The space group is *Cmma*. Approximate atom positions are shown in Table II. Figure 5b is a simulated image for β-V_6O_{13} under the beam incidence along the $[001]_\beta$. This interprets the observed image fairly well.

Discussion

In the present study, we succeeded in imaging the V-atom rows in V_6O_{13} as well as the tunnels in its structure by using the UHV-HR-1 MV EM. Although the radiation damage took place under a strong electron irradiation, it could be avoided by reducing the beam intensity and exposure

TABLE II

TENTATIVE CRYSTALLOGRAPHIC DATA OF β-V_6O_{13}

Monoclinic, space group *Cmma* (No. 67)
Lattice parameters: $a = 1.1922$, $b = 1.9912$, $c = 0.3680$ nm
Number of formula unit in the unit cell: $M = 4$
Atom positions: (0, 0, 0; 1/2, 1/2, 0) +
V(1) at 16(*o*) with $x = 0.15$, $y = 0.07$, $z = 0.75$,
V(2) at 8(*n*) with $x = 0.14$, $z = 0.75$,
O(1) at 16(*o*) with $x = 0.18$, $y = 0.05$, $z = 0.25$,
O(2) at 16(*o*) with $x = 0.14$, $y = 0.15$, $z = 0.75$,
O(3) at 8(*n*) with $x = 0.18$, $z = 0.25$,
O(4) at 8(*m*) with $x = 0.05$, $z = 0.75$,
O(5) at 4(*g*) with $z = 0.75$

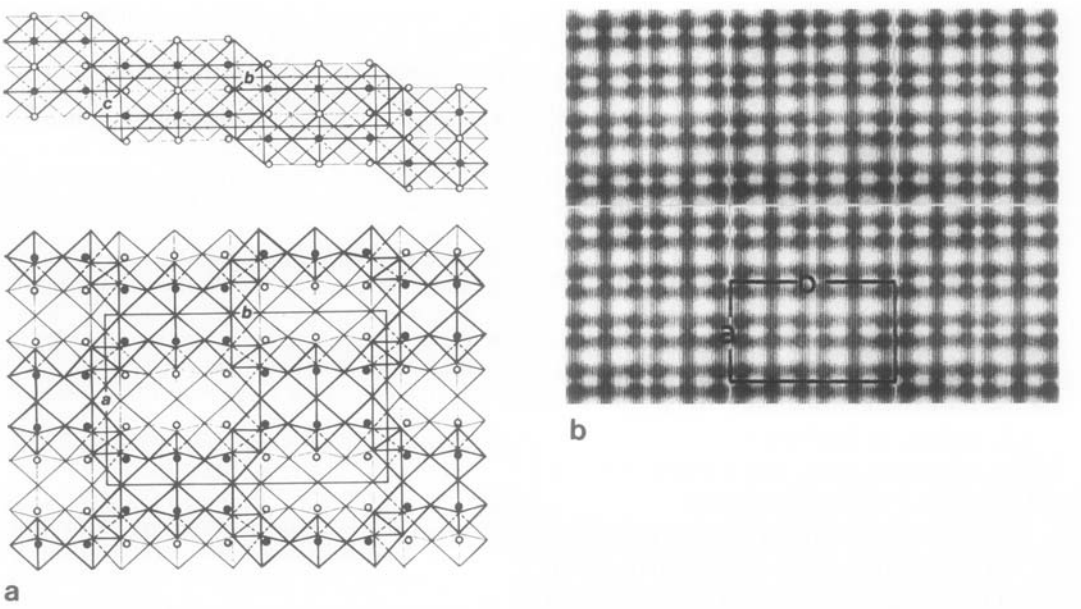

FIG. 5. (a) Crystal structure of β-V_6O_{13}. Upper figure: [100] projection. Lower figure: [001] projection. Open and solid circles represent V atoms, while O atoms are at the corners of octhadra. (b) Simulated image of β-V_6O_{13}. Incident beam direction is [001].

time. The effect of contamination and the resulting reduction of V_6O_{13} (*11*) were not observed. This is due to a clean vacuum greater than 1×10^{-5} Pa around the specimen.

The image simulation showed that the neutral model interpreted more satisfactorily the observed image than the ionized model. This might be thought to contradict with Gossard *et al.*'s results from the nuclear magnetic moment measurement of various vanadium oxides, where V atoms in metallic V_6O_{13} are thought to be in an intermediate state between the neutral and ideally ionized states (*20*). However, Hirotsu *et al.*'s electron diffraction measurement of crystal structure factor of metallic V_7O_{13} (*21*) has shown that the scattering amplitude for V atom is close to that of the neutral atom in a low scattering angle region ($\sin\theta/\lambda < 1\ \text{nm}^{-1}$) and approaches that of an ionized atom (approximately V^{3+}) with increasing scattering angle. Roughly speaking, the atomic scattering amplitude in the low scattering angle region reflects the distribution of outer electrons, while that in the higher scattering angle region does the distribution of inner electrons. Therefore, we can assume that the electron distribution in V atom in V_7O_{13} resembles the electron distribution in the neutral atom for the outer electrons and the electron distribution in the ionized atom for the inner electrons. The same consideration may be applied to the present V_6O_{13} in the metallic state. The magnetic moment measurements provide information on the rather localized 3*d* electron distribution, but in electron micrographs, the distribution of rather nonlocalized valence electrons contributes remarkably to the image formation through the low-order reflections. This is considered to be the reason why the image simulation based on the neutral model interpret the image more satisfactorily than the ionized model.

A modification of V_6O_{13}, which we named β-V_6O_{13}, was imaged, and its struc-

ture model was proposed. This model is different from the normal α-V_6O_{13} structure only in the direction of *CS* plane. The positional parameters of constituent atoms are approximate. Although a more refined structure analysis must be made, this model is considered to be fairly reliable, since the simulated image can interpret the observed image and also the model can interpret the optically transformed patterns of recorded images. It seems worthwhile to mention the following fact: while M_2O_5 (*M*: W, V) (*22*) and *M*-Nb_2O_5 (*23*) take the so-called 4 × 4 block structure, and M_3O_7 takes the 3 × 3 block structure (*24*), the present β-V_6O_{13} takes the 2 × 3 block structure.

Sata and Ito (*25*) reported a modification of V_6O_{13} named as the intermediate compound C. According to their X-ray powder diffraction pattern, it is cubic with lattice parameter $a = 0.880$ nm. Trials have been made to identify the present β-V_6O_{13} with their intermediate compound C without success. This is because their precision of X-ray data is too low for identification.

In contrast to the cases of V_6O_{11} and V_7O_{13} (*5*, *6*), the microsyntactic intergrowth of neighboring phases was not observed. This may be ascribed to the difference in the specimen preparation condition. In the present case, the reaction time to form V_6O_{13} was very long and the produced specimen was cooled slowly.

Acknowledgments

The authors express their thanks to Dr. Y. Hirotsu, Technological University of Nagaoka, for his assistance and discussions during this study. This work was partly supported by the Grant-in-Aids for Cooperative Research from the Ministry of Education, Science and Culture, Japan.

References

1. K. Kosuge, *J. Phys. Chem. Solids* **28,** 1613 (1967).
2. A. D. Wadsley, *Acta Crystallogr.* **10,** 261 (1957).
3. K. Kawashima, K. Kosuge, and S. Kachi, *Chem. Lett.* 1113 (1957).
4. Y. Hirotsu, S. P. Faile, and H. Sato, *Mater. Res. Bull.* **13,** 895 (1978).
5. Y. Hirotsu, and H. Sato, *Mater. Res. Bull.* **15,** 41 (1980).
6. Y. Hirotsu, Y. Tsunashima, S. Nagakura, H. Kuwamoto, and H. Sato, *J. Solid State Chem.* **43,** 33 (1982).
7. F. Aebi, *Helv. Acta* **31,** 8 (1948).
8. K. A. Wilhelmi, K. Waltersson, and L. Kihlborg, *Acta Chem. Scand.* **25,** 2675 (1971).
9. H. G. Bachmann, F. R. Ahmed, and W. H. Barnes, *Z. Kristallogr.* **115,** 110 (1961).
10. S. Horiuchi, and Y. Matsui, *Philos. Mag.* **30,** 777 (1974).
11. S. Horiuchi, M. Saeki, and Y. Matsui, *Acta Crystallogr. Sect. A* **31,** 660 (1975).
12. G. Honjo, K. Yagi, K. Takayanagi, S. Nagakura, S. Katagiri, M. Kubozoe, and I. Matsui, "Electron Microscopy—1980" (Proceedings, 6th International Conference on High Voltage Electron Microscopy, Antwerp, Sept. 1–3, 1980), Vol. 4, p. 22 (1980).
13. K. Yagi, K. Takayanagi, S. Nagakura, K. Kobayashi, G. Honjo, M. Kubozoe, K. Shii, I. Matsui, S. Katagiri, and T. Yanaka, "Proceedings, 10th International Congress on Electron Microscopy (Hamburg, Aug. 17–24, 1882)," p. 375.
14. J. M. Cowley, "Diffraction Physics," Chap. 11, North-Holland, Amsterdam (1975).
15. S. Nagakura, M. Kikuchi, and S. Oketani, *Acta Crystallogr.* **21,** 1009 (1966).
16. S. Nagakura, *J. Phys. Soc. Jpn.* **25,** 488 (1968).
17. S. Nagakura, and K. Tanehashi, *J. Phys. Soc. Jpn.* **25,** 840 (1968).
18. S. Nagakura, and N. Otsuka, *J. Phys. Soc. Jpn.* **39,** 1047 (1968).
19. G. R. Antis, D. E. Linch, A. F. Moodie, and M. A. O'Keefe, *Acta Crystallogr. Sect. A* **29,** 138 (1973).
20. A. Gossard, F. J. Di Salvo, L. C. Erich, J. P. Remeika, H. Yasuoka, K. Kosuge, and S. Kachi, *Phys. Rev. B* **10,** 4178 (1974).
21. Y. Hirotsu, H. Sato, and S. Nagakura, "Modulated Structures—1979" (J. M. Cowley, J. B. Cohen, M. B. Salamon, and B. J. Wuensch, Eds.), AIP Conf. Proc. No. 53, p. 75 (1979).
22. M. Israelsson, and L. Kihlborg, *Ark. Khim.* **30,** 129 (1968).
23. W. Mertin, S. Andersson, and R. Gruehn, *J. Solid State Chem.* **1,** 419 (1970).
24. J. Darriet, and J. Galy, *J. Solid State Chem.* **4,** 357 (1972).
25. T. Sata, and Y. Ito, *Kogyo Kagaku Zasshi* **71,** 648 (1968).